Computer Methods and Programs in Biomedicine 254 (2024) 108307

Contents lists available at ScienceDirect

Computer Methods and Programs in Biomedicine

journal homepage: www.sciencedirect.com/journal/computer-methods-and-programs-in-biomedicine

Influence of genetic mutations to atria vulnerability to atrial fibrillation: An in-silico 3D human atria study

Rebecca Belletti [a,*], Joaquín Osca [b], Lucia Romero Perez [a,1], Javier Saiz [a,1]

[a] Centro de Investigación e Innovación en Bioingeniería, Universitat Politécnica de València, Camino de Vera, s/n, 46022,Valencia, Spain
[b] Electrophysiology Section, Cardiology Department, Hospital Universitari i Politecnic La Fe, Avinguda de Fernando Abril Martorell, 106, Quatre Carreres, 46026, València, Spain

ARTICLE INFO

Keywords:
Atrial fibrillation
3D in-silico modelling
Genetic mutations
Arrhythmia inducibility
Atria vulnerability

ABSTRACT

Background and Objective: Personalized 3D computer models of atria have been extensively implemented in the last yearsas a tool to facilitate the understanding of the mechanisms underlying different forms of arrhythmia, such as atrial fibrillation (AF). Meanwhile, genetic mutations acting on potassium channel dynamics were demonstrated to induce fibrillatory episodes in asymptomatic patients. This research study aims at assessing the effects and the atrial susceptibility to AF of three gain-of-function mutations – namely, KCNH2 T895M, KCNH2 T436M, and KCNE3-V17M – associated with AF outbreaks, using highly detailed 3D atrial models with realistic wall thickness and heterogenous histological properties.

Methods: The 3D atrial model was generated by reconstructing segmented anatomical structures from CT scans of an AF patient. Modified versions of the Courtemanche human atrial myocyte model were used to reproduce the electrophysiological activity of the WT and of the three mutant cells. Ectopic foci (EF) were simulated in sixteen locations across the atrial mesh using an S1-S2 protocol with two S2 basic cycle lengths (BCL) and eleven coupling intervals in order to induce arrhythmias.

Results: The three genetic mutations at 3D level reduced the APD_{90}. The KCNE3-V17M mutation provoked the highest shortening (55 % in RA and LA with respect to WT), followed by KCNH2 T895M (14 % in RA and 18 % LA with respect to WT)and KCNH2 T436M (7 % in RA and 9 % LA with respect to WT). The KCNE3-V17M mutation led to arrhythmia in 67 % of the cases simulated and in 94 % of ectopic foci considered, at S2 BCL equal to 100 ms. The KCNH2 T436M and KCNH2 T895M mutations increased the vulnerability to AF in a similar way, leading to arrhythmic episodes in 7 % of the simulated conditions, at S2 BCL set to 160 ms. Overall, 60 % of the arrhythmic events generated arise in the left atrium. Spiral waves, multiple rotors and disordered electrical pattern were elicited in the presence of the KCNE3-V17M mutation, exhibiting an instantaneous mean frequency of 7.6 Hz with a mean standard deviation of 1.12 Hz. The scroll waves induced in the presence of the KCNH2 T436M and KCNH2 T895M mutations showed steadiness and regularity with an instantaneous mean frequencies in the range of 4.9 – 5.1 Hz and a mean standard deviation within 0.19 – 0.53 Hz.

Conclusions: The pro-arrhythmogenicity of the KCNE3-V17M, KCNH2 T895M and KCNH2 T436M mutations was studied and proved on personalized 3D cardiac models. The three genetic mutations were demonstrated to increase the predisposition of atrial tissue to the formation of AF-susceptible substrate in different ways based on their effects on electrophysiological properties of the atria.

Abbreviations: EF, ectopic foci; BCL, basic cycle length; CI, coupling intervals.

Mathematical symbols: σ_L: longitudinal conductivity; σ_T: transversal conductivity; α_x: forward rate constant for gating variable x; β_x: backward rate constant for gating variable x

* Corresponding author.
E-mail address: rbelletti@ci2b.upv.es (R. Belletti).

[1] JS and LRP share senior authorship.

https://doi.org/10.1016/j.cmpb.2024.108307
Received 15 January 2024; Received in revised form 21 June 2024; Accepted 24 June 2024
Available online 26 June 2024

1. Introduction

Atrial fibrillation (AF) is a cardiac arrhythmia characterized by asynchronous, high frequency excitations of the atria, which result in inefficient atrial contractions and thus ineffective pumping of blood throughout the body districts. AF is well known to be the most common sustained cardiac rhythm disorder affecting 2–4 % of adult population, expected to increase in the coming decades with pandemic proportions [1]. Even if it is not a lethal pathology itself, AF is associated with a higher risk of thromboembolic strokes and mortality, cognitive and psychological decline, frequent hospitalization and to an overall impaired quality of life. Many studies demonstrated that the occurrence of AF is determined by the presence of a substrate prone to the formation of AF episodes and that the presence and characteristics of such substrate may depend on the combination of unmodifiable and modifiable risk factors. Age, sex, race, cardiovascular and metabolic diseases, respiratory conditions, obesity and hypertension are just some of the risk factors that were demonstrated to induce electrical and structural remodelling, promoting substrate generation and increasing susceptibility to AF [1–3]. Among the unmodifiable risk factors, heritability was demonstrated to play a determinant role in the outbreak of fibrillatory events in apparently healthy subjects [4,5]. Isolation of genes and genome-wide association studies allowed to identify specific genetic mutations and, in particular, the ones affecting the genes that encode the potassium channel protein structures turned out to lead to the most serious forms of both familial and lone AF [6,7]. Such genetic defects were demonstrated to impair the normal functioning of K^+ channels in experimental studies by acting directly on the repolarization phase in cardiac cells' electrophysiology, thus affecting the action potential duration, the cell excitability and the conduction velocity [8,9]. In such a context, computational models of cardiac cells electrophysiology have been used to investigate in deep into the complex dynamics and mechanisms behind mutation-related AF episodes [10]. Many simulation studies reproduced the conditions above-mentioned by introducing the mutant effects into pre-existent atrial cellular models from the experimental data. The consequences of the presence of genetic mutations affecting the genes responsible for the encoding of I_{Ks}, I_{K1} and I_{Kr} ionic channels were investigated in several research works. In these works, the mutation – related changes produced in the experimental data were integrated into the corresponding ionic current formulations, thus modelled and simulated using multiscale cardiac cell models [11–16]. The characterization of the genetic mutations' possible effects and implications were investigated at cellular level and tissue level, even though just a slight characterization was given by using homogeneous 3D human atrial models. In this study, the effects of three gain-of-function mutations – KCNH2 T436M, KCNH2 T895M, KNCE3-V17M – affecting I_{Kr} and I_{to} and previously studied at single cell and tissue level [17] are investigated by using computer simulations of realistic and heterogeneous 3D atrial models. The characterization of the mutations' effects on 3D human atrial geometries was carried out by employing a specifically designed induction protocol applied on many locations throughout the atrial surface. Highly detailed 3D computer models revealed to be a valuable tool and can help in gaining a more comprehensive understanding of the mechanisms behind arrhythmias by revealing complex underlying dynamics that cannot be accounted for on 0D and 2D simulations, and therefore, can help in driving patient-tailored therapeutical strategies and ablation procedures [18].

The aim of the study is to provide a comprehensive assessment of the effects of the genetic mutations on the electrical properties of the atria using a highly detailed patient-specific geometry with realistic wall thickness and fibre orientation. Moreover, the vulnerability to AF was determined by applying a stimulation protocol to induce arrhythmias in focal sources homogeneously distributed among the regions of the 3D model.

2. Materials and methods

2.1. 3D wild-type atrial model

The 3D atrial model used in this study was built and developed by segmenting the anatomical structures of the atria from CT scans of a former AF patient. The patient was suffering from arterial hypertension, paroxysmal AF that developed into persistent AF and showed slightly dilated atria. The 3D hexahedral geometrical mesh representing the human atria is a highly detailed bi-atrial model composed of 1.893.314 nodes and 1.655.986 elements, with a spatial resolution of 330 μm. The geometry is characterized by regionally heterogenous realistic wall thickness and by 45 regions with different histological properties and fibre orientation [19,20], as shown in Fig. 1A. Moreover, eleven different conduction velocities were defined on the mesh by tuning longitudinal conductivity values (σ_L) and anisotropy ratios ($AR = \sigma_T/\sigma_L$), what gives rise to eleven types of tissue, namely: CT, RA / LA, CS, RFO (FO ring), Isthmus, PM / BBRA, FO / CS bridges, BBLA, PV, SAN, as shown in Fig. 1B (see Table S1 in Supplementary Materials for details). More details about the atrial geometry generation are given in the Supplementary Materials. A modified version of a well-established mathematical model was chosen to reproduce the cardiac electrophysiology of a single cell in healthy conditions, the Courtemanche-Ramirez-Nattel (CRN) human atrial model. To include the formulation of the potassium-activated acetylcholine (I_{KACh}) current, with [ACh] = 0.005 μM [21,22] was included to simulate the influence of the autonomic nervous system on the repolarization phase of cardiac electrical activity, both in healthy and in pathological conditions [23,24]. Furthermore, the electrophysiological heterogeneity was considered by scaling channels' conductances to account for the heterogeneous electrical properties of atrial regions, resulting in nine different atrial models, similarly to a previous study [25]. Specifically, the nine atrial models are BBLA, MVR, PV, LAA, LA, RAA, TVR, BBRA/CT, RA/PM and are shown in Fig. 1C.

2.2. 3D mutant atrial models

Three mutant versions of the atrial model were considered in this work, one for each mutant case (KCNH2 T436M, KCNH2 T895M, KCNE3-V17M). They were obtained by reproducing the altered effects of the genetic mutations in the I_{Kr} and I_{to} current formulations of the Courtemanche-Ramirez-Nattel model, which represent the wild-type version, as in [17] and as shown in the Eqs. (1) to (6) and in Table 1. Five parameters (p_0 to p_4) were included in the I_{Kr} formulation and, other five parameters (p_5 to p_9) were incorporated in the I_{to} current formulation.

$$\alpha_{xr} = 0.0003\ \frac{V+14.1}{1-\exp^{\frac{V+14.1}{-5}}} \tag{1}$$

$$\beta_{xr} = p_0 \cdot 7.3898 \cdot 10^{-5}\ \frac{V-3.3328+p_1}{\exp^{\frac{V-3.3328+p_1}{5.1237 \cdot p_2}}-1} \tag{2}$$

$$I_{Kr} = C_m \cdot p_3 \cdot g_{Kr} \cdot xr\ \frac{V-E_K}{1+\exp^{\frac{V+15}{22.4 \cdot p_4}}} \tag{3}$$

$$\alpha_{oi} = \frac{p_5}{18.53+\exp^{\frac{V+113.7}{10.95 \cdot p_6}}} \tag{4}$$

$$\beta_{oi} = \frac{p_7}{35.56+\exp^{\frac{V+1.26}{-7.44 \cdot p_8}}} \tag{5}$$

$$I_{to} = C_m \cdot p_9 \cdot g_{to} \cdot oi \cdot oa^3 (V-E_K) \tag{6}$$

The effects induced by the presence of the three genetic mutations on

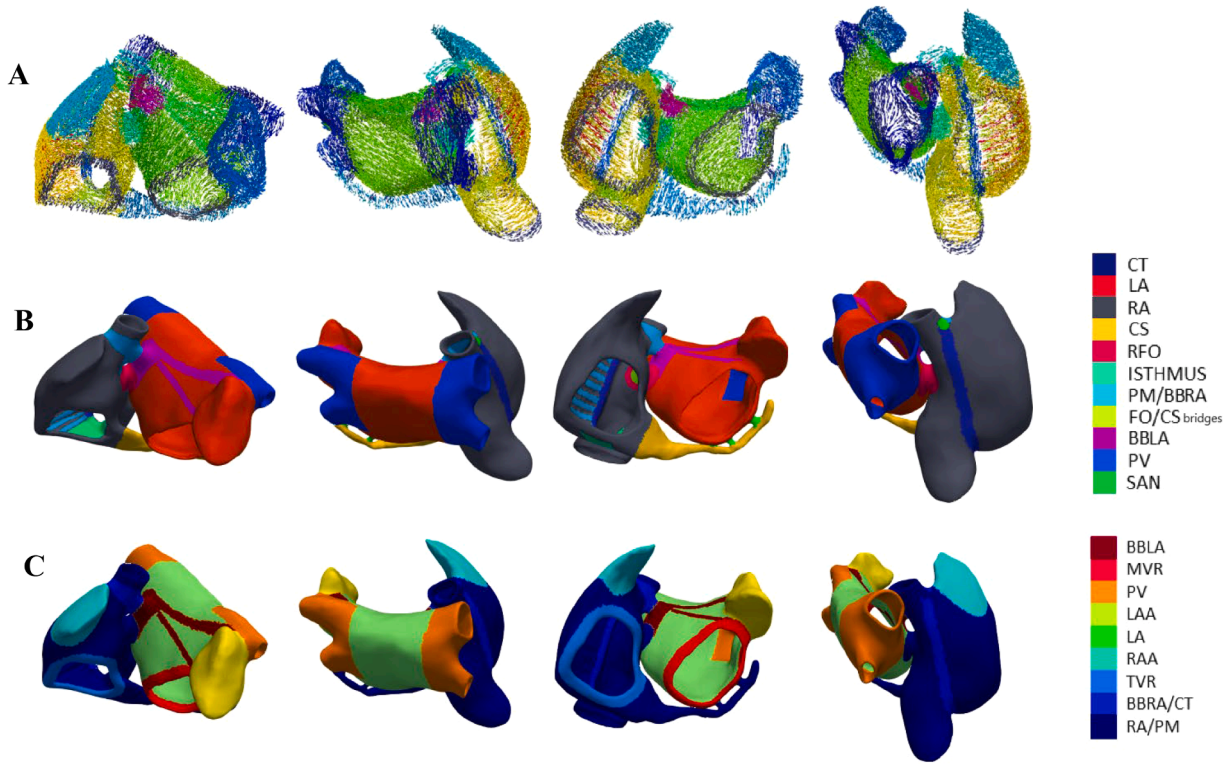

Fig. 1. 3D geometrical model. Views of the 3D geometrical model of the atria. **A)** Coloured 3D geometry showing the 45 histologically different regions and showing principal fibre directions. **B)** 3D atria color-coded by the eleven types of tissue – namely CT, LA, RA, CS, RFO, Isthmus, PM/BBRA, FO/CS bridges, BBLA/FO union, PV, SAN. **C)** 3D mesh divided into nine regions, one for each ionic model employed in the study – namely, BBLA, MVR, PV, LAA, LA, RAA, TVR, BBRA/CT, RA/PM.

Table 1
Parameters' values that reproduce the effects produced by the mutations.

	I_{Kr}			I_{to}	
Parameter	KCNH2 T895M	KCNH2 T436M	KNCE3-V17M	Parameter	KCNE3-V17M
p_0	2.134	1.08	0.51	p_5	2
p_1	51.14	46.96	–	p_6	1.87
p_2	3.49	4.64	–	p_7	8.14
p_3	1.99	1.41	6.18	p_8	0.68
p_4	–	–	0.71	p_9	12.56

the electrophysiological properties of atrial cells were analysed in detailed in a previous in-silico study providing the impact on ionic currents, action potential durations and restitution curves. The KCNH2 T436M / KCNH2 T895M mutations provoked a 29 % / 63 % increase in the WT I_{Kr} peak value in RA, and thus a reduction of the WT APD_{90} value of the 9 % / 18 %, respectively. The KCNE3- V17M mutation led to an increased of the 113 % of the WT I_{Kr} peak value and of the 252 % of the WT I_{to} peak value in RA; this resulted into a shortening of the 46 % of the WT APD_{90} value. More details can be found in [17].

2.3. Sinus rhythm stimulation

The nine ionic models shown in Fig. 1C, in the presence of each genetic mutation (KCNH2 T436M, KCNH2 T895M and KCNE3-V17M) and in absence of pathological conditions (WT), were stabilized at cellular level by applying 60 pulses at 1 Hz of frequency using a current amplitude of 20 pA/pF for 2 ms to get the initial conditions of the nodes of the 3D models. Then, cellular models were introduced into 3D model and it was stabilized by applying 5 stimuli with BCL of 1000 ms at the SAN region in order to smooth the electrical differences among regions. The activation times of the atria are shown in Figure S1, S2, S3 and S4 of the Supplementary Materials. The APD_{90} values were computed and extracted at the 4th SAN stimulation for each ionic model to understand the effects of the mutants on the electrophysiological properties of the 3D models during sinus rhythm stimulation.

2.4. S1-S2 stimulation protocol

An S1-S2 stimulation protocol was applied to assess atria vulnerability. Fig. 2A illustrates the last S1 beat applied to the SAN and the 10 stimuli of the S2 train applied to a circular region (radius = 0.2 cm), mimicking an ectopic focus (EF). As many as sixteen different locations were defined and homogeneously distributed across the atrial mesh, considering an inter-point distance of approximately 3.5 cm among their centres. The sixteen EF location are represented in panels B, C, D, and E of Fig. 2 and are named: RA sup wall, RA inf wall, under RIP / FO, CT, IVC, LA roof, LA wall ant, LA wall post, LAA, RAA, MVR, TVR, TVR/CS, CS, RSPV and mid LPVs. Since a wide range of effective refractory periods (ERPs) was observed during sinus rhythm simulations, the S2 stimuli were applied using two different BCLs – 100 ms and 160 ms. The simulations were run for 3.5 s in case of S2–BCL equal to 100 ms and for 4 s in case of S2–BCL equal to 160 ms. This allowed to observe the evolution of the ectopic stimulation during the 2 s following the end of the S2 train of stimuli. Eleven coupling intervals (CI) were used varying its value ranging from 0 ms to 200 ms with 20ms–increments were used, the APD_{97} of the last sinus beat (S1) being considered as the starting time. This protocol allowed to reproduce multiple firing sources that cover the atrial geometry and to simulate realistic episodes of spontaneous ectopic bursts. In this study, a total number of 1408 simulations were performed as a result of the combination of four atrial ionic models (three mutated and the WT case), sixteen ectopic locations (Fig. 2 panels B, C, D, E), two BCLs (100 ms and 160 ms) and eleven CIs. Only the

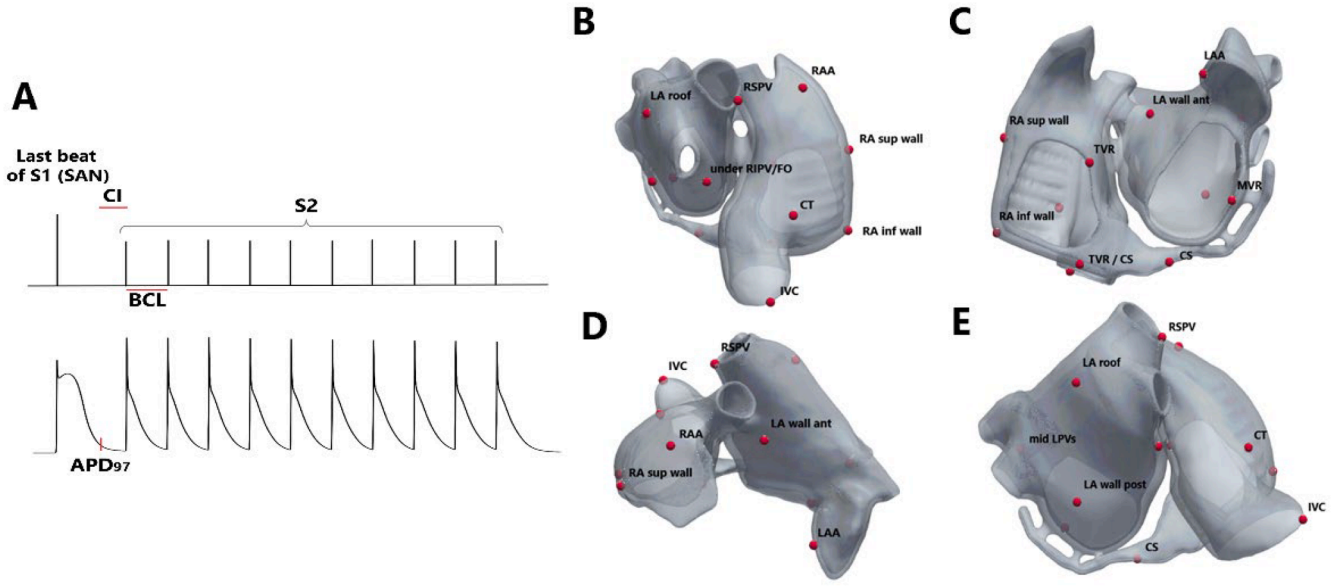

Fig. 2. Stimulation protocol and EF locations. A) Stimulation protocol representation showing the coupling interval (CI), the basic cycle length (BCL), the train of 10 stimuli applied to each EF (S2) and the action potential duration at 97 % of repolarization (APD_{97}); **B), C), D)** and **E)** EF location and distribution across the patient-specific atrial mesh in different atrial views.

arrhythmias that completed at least 2 cycles around the atria were presented in this work. Arrhythmia generation was analysed with respect to type of genetic mutation, to the number of EF locations and to their positions on the atria. Finally, for each sustained AF episode induced, the voltage time courses were extracted from two nodes of the mesh, one placed in RA and one placed in LA. Then, the instantaneous frequency was computed as the inverse of the interval between two consecutive voltage peaks in the last 1500 ms of the APs time course. The mean and standard deviation of the instantaneous frequencies obtained for each sustained arrhythmia was then computed in both nodes, resulting in one single value for the mean and standard deviation for each episode observed. For each mutation, the mean of the overall mean values and the mean of the overall standard deviation values were computed. This analysis allowed the characterization of the complexity of the elicited arrhythmic patterns at low computational costs.

2.5. 3D human atrial simulations

The monodomain formalism was solved using the Elvira software (Heidenreich et al., 2010) with a time step of 0.01 ms (Ferrer et al.,

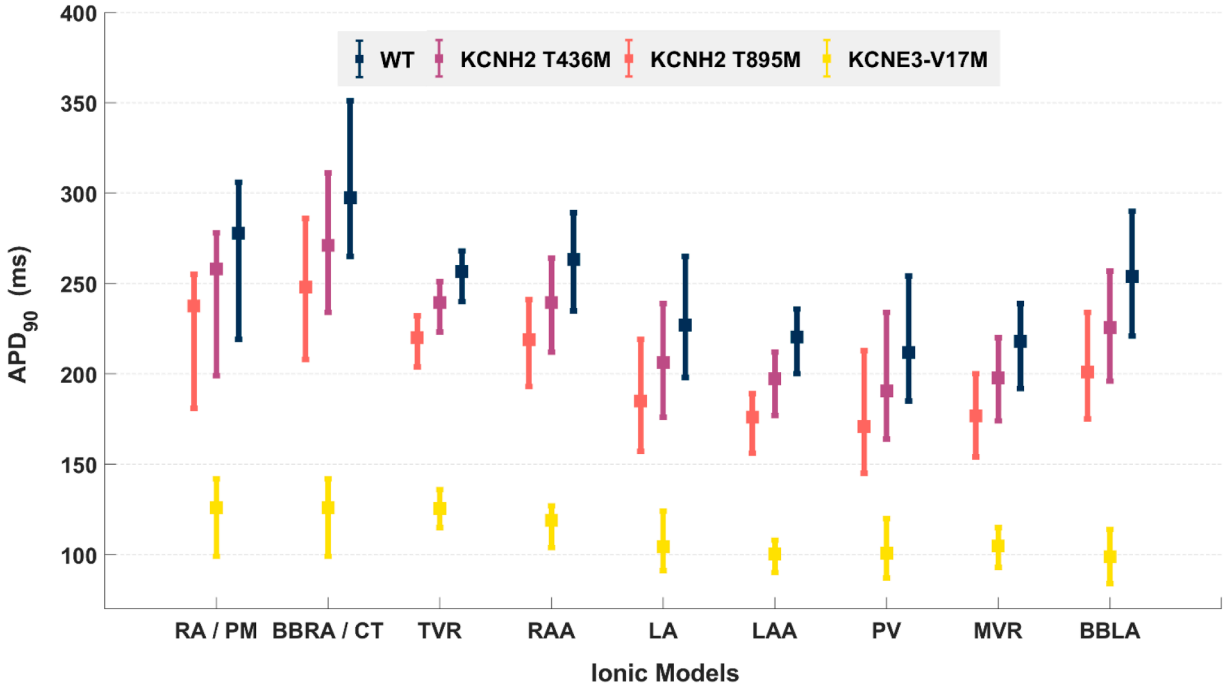

Fig. 3. Mutation effects on 3D model. Error bars representing the mean values and ranges of APD_{90} (ms) for the nine ionic model (x-axis) – BBLA, MVR, PV, LAA, LA, RAA, TVR, BBRA/CT, RA/PM – color-coded by the case under study – dark blue for WT, purple for KCNH2 T436M, orange red for KCNH2 T895M and yellow for KCNE3-V17M. The range is given by the highest and the lowest value of APD_{90} for that region.

2015; Martinez-Mateu et al., 2018). The 3D atrial geometry was stimulated by applying a 2 ms-excitation current of amplitude 28 pA/pF both to the SAN and to the EF.

3. Results

3.1. Effects of the mutations on a 3D atrial geometry

The sinus rhythm simulations were run by pacing 5 beats to the SAN region of the 3D atrial model using a BCL of 1000 ms. The APD_{90} values were then computed, for the last beat, both in the presence of the genetic mutations – KCNH2 T436M, KCNH2 T895M and KCNE3-V17M – and in healthy conditions (WT) in every node of the mesh. Fig. 3 illustrates the overall resulting effects of the presence of the genetic mutants compared to the healthy condition. The values of the APD_{90} are presented for each ionic model in terms of means and ranges and are color-coded by the four atrial models above-mentioned. The three genetic mutations provoke a shortening of the mean values of the APD_{90} with respect to the WT case (dark blue). In particular, the KCNH2 T436M mutation (purple) is the one that affects the APD_{90} mean values to the least extent, followed by the KCNH2 T895M mutation (orange red). Overall, the reductions of the APD_{90} are fairly homogeneous in all the nine electrophysiological regions. On the contrary, the KCNE3-V17M mutation shortened the APD_{90} the most and reduced the dispersion of the APD_{90} within the same region and among all the nine regions. For example, the mean value of the APD_{90} in the presence of the KCNE3-V17M mutation is reduced to the 55 % with respect to the WT case both in RA and LA regions (152 ms and 122 ms, respectively). Fig. 4 displays the electrical propagation in sinus rhythm at four time instants –namely 35 ms, 70 ms, 105 ms and 140 ms – in the four atrial models under study. The electrical wave scrolling across the atrial mesh demonstrates qualitatively the fast repolarization in presence of the three mutations, mild for the KCNH2 T436M and the KCNH2 T895M mutations and much evident for the KCNE3-V17M mutation.

3.2. Effects of the mutations on temporal vulnerability to arrhythmias

A number of 1408 computer simulations were performed by using the stimulation protocol described in Section 2.4 and depicted in Fig. 2A. Sixteen different locations were paced to reproduce the effects of ectopic bursts in the atrial geometry in order to assess atrial susceptibility to AF induction both in the presence of three genetic mutations – KCNE3-V17M, KCNH2 T895M, KCNH2 T436M – and in the healthy conditions. Fig. 5A depicts the number of CIs for which an arrhythmic episode was observed after the ectopic stimulation with S2 BCL equal to 100 ms (full coloured bars) and with S2 BCL equal to 160 ms (dashed coloured bars). The number of CIs leading to arrhythmias is sorted by EF location in the atria (respectively, LA and RA locations along y-axis) and by the atrial model (dark blue for WT, purple for KCNH2 T436M, orange red for KCNH2 T895M and yellow for KCNE3-V17M). Fig. 5B shows the overall percentage of arrhythmic behaviour for WT and for each mutation. When S2 BCL is set to 100 ms (Fig. 5A, full coloured bars), the KCNE3-V17M mutation resulted to be the most pro arrhythmogenic mutation among the three studied leading to arrhythmia in 67 % of the simulated cases. In fact, the KCNE3-V17M mutation induced arrhythmic patterns in 15 of the 16 EF sites, which is close to the 94 % of the considered locations. The highest number of arrhythmias were generated in the EF named TVR/CS, CS and mid LPVs. Of the 15 EF leading to re-entry, 40 % were placed in RA, 27 % in LA, 13 % around the valves (MVR/TVR) and 20 % in the PV and LAA regions. The results in Fig. 5A (full coloured bars) also show a significantly lower impact of the KCNH2 T895M and KCNH2 T436M mutations when S2-BCL is set to 100 ms. The KCNH2 T436M mutation led to arrhythmic patterns when the ectopic stimulation was applied in the LA posterior wall (LA post wall) and to the LA roof. Similarly, just the EF located in the TVR/CS region resulted in an arrhythmic pattern in the presence of the KCNH2 T895M mutation. Finally, in absence of genetic mutations (WT case), three EF, named LA roof, RSPV and RIPV/FO, led to forms of arrhythmias. For those cases, two of the foci were placed in LA and the other one in the PV regions. When BCL is set to 160 ms the mutation showing the highest pro-arrhythmogenic outcomes is the KCNH2 T436M, closely followed by the KCNH2 T895M. The former mutation in fact led to the formation of arrhythmic patterns in 6 EF sites (namely, LAA, MVR, mid LPVs, RSPV, LA roof and under RIPV/FO), placed around the valves, in LA appendage, in the left atrium and in the PV region. The latter mutation, KCNH2 T895M, induced an arrhythmia in five stimulated EF locations, which were uniformly distributed among the mid LPV, the MVR, the TVR/CS region, the LA posterior wall and the LAA regions. No arrhythmia was induced either in presence of the KNCE3-V17M mutation or in the WT healthy scenario case when the EF were stimulated with the BCL set to 160 ms. In addition, no arrhythmic events were observed in the RAA region at all. Fig. 5B shows a summarized overview of the results. Most arrhythmias were elicited when the BCL was set to 100 ms and at this BCL almost the 70 % of the arrhythmias were generated in the presence of the mutation KCNE3-V17M, while only the 3 % were induced in the presence of the KCNH2 T436M mutation and in healthy case and just for almost 1 % of the cases in the presence of the KCNH2 T895M mutation. On the other hand, when the BCL was set to 160 ms, the number of arrhythmic episodes was much smaller, and they were elicited only under the effects of the KCNH2 T436M mutation (7 %) and KCNH2 T895M mutation (7 %). In addition, the characterization of the complexity of the arrhythmic AF patterns is provided by computing the instantaneous frequency. In particular, as mentioned above, the mean and standard deviation of the instantaneous frequencies obtained for each sustained case was computed in the two nodes, in RA and LA, resulting in on single value of mean and standard deviation for each episode observed. A number of 13 sustained AF cases were observed for the KCNH2 T436M and the KCNH2 T895M mutations and 102 for the KCNE3-V17M mutation. Therefore, the mean of the overall mean values and the mean of the overall standard deviation values of the sustained episodes have been obtained and presented in panel C of Fig. 5. The sustained arrhythmias provoked by the presence of the KCNE3-V17M mutation exhibited an instantaneous frequency mean of 7.6 Hz, with a standard deviation of 1.12 Hz; such results reflect the rapid and chaotic behaviour of such mutation. Meanwhile, the AF episodes caused by the presence of the KCNH2 T895M and KCNH2 T436M mutations showed an instantaneous frequency mean within the range of 4.9 – 5.1 Hz and a standard deviation within the range of 0.19 – 0.53 Hz, indicating more regular and steady patterns.

Examples of the temporal evolution of the arrhythmic events and of the action potentials are shown in Fig. 6 for the three mutations. Figures S5, S6, S7 and the videos “KCNH2 T436M”, “KCNH2 T895M” and “KCNE3-V17M” of Supplementary Materials show more in details the evolution of the scroll waves. The APs correspond to a mesh node located in the left atrium roof. The spiral waves illustrated in Fig. 6 and in the Supplementary Materials were induced by stimulating the three 3D pathological atrial models in the same EF location, mid LPV, and the CIs and BCLs depended of the mutation. The arrhythmia elicited in the presence of the KCNE3-V17M mutation (Fig. 6 panel c and Figure S7) is characterized by the generation of multiple spiral waves and rotors, moving chaotically around the atrial walls, eventually colliding with other re-entries or anatomical structures. Meanwhile, more regular and steady behaviour is shown in the arrhythmias provoked by the KCNH2 T436M (Fig. 6 panel a and Figure S5) and KCNH2 T895M (Fig. 6 panel b and Figure S6) mutations, with macro re-entries and short living single rotor. The characteristics of the AF patterns presented in these three examples reflect the results of the instantaneous frequency analysis for which more rapid and chaotic patterns are provoked by the KCNE3-V17M mutation, while more regular behaviour is shown in the presence of the KCNH2 T436M and KCNH2 T895M mutations.

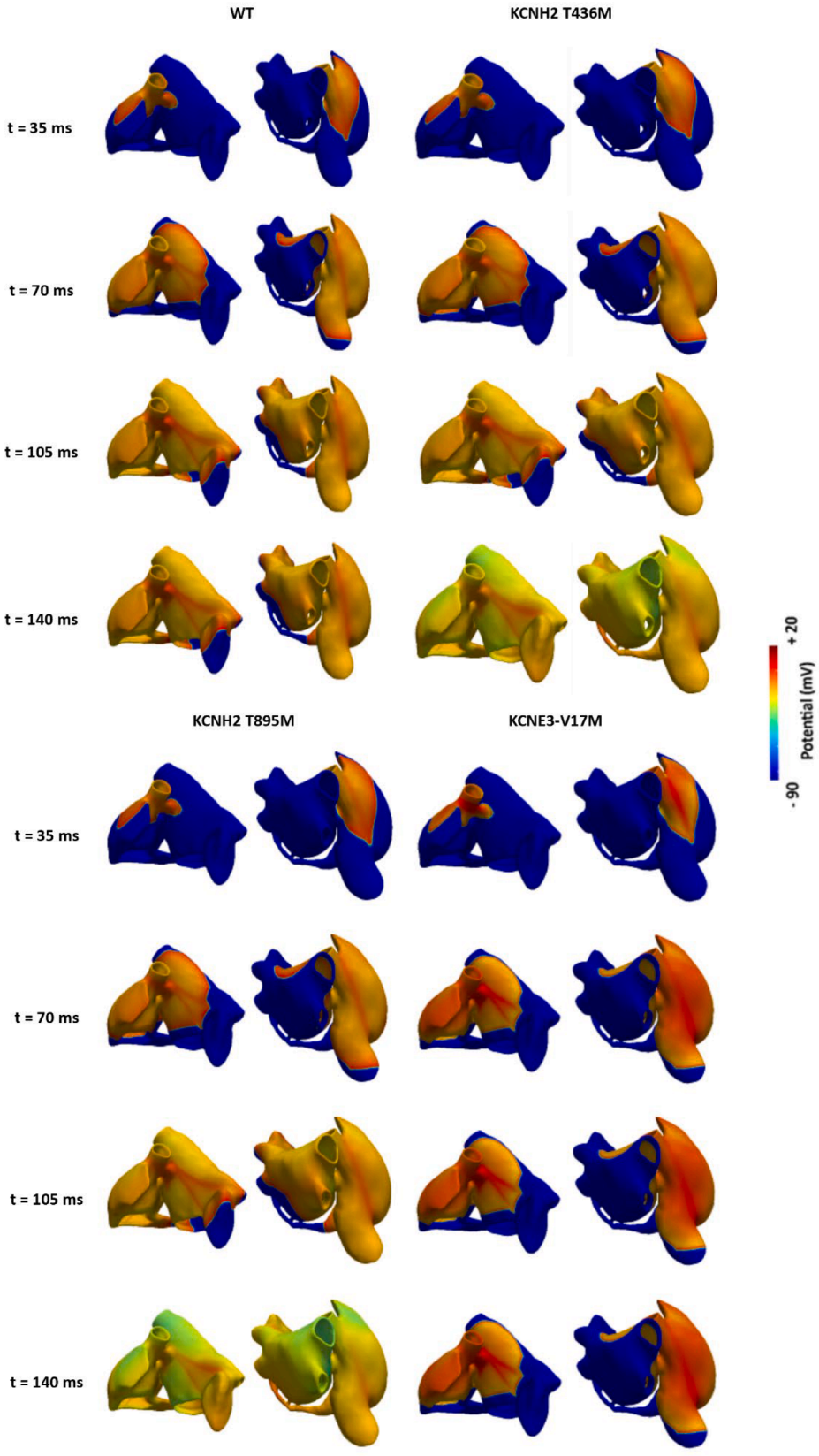

Fig. 4. Electrical propagation in sinus rhythm for WT, KCNH2 T436M, KCNH2 T895M and KCNE3-V17M.

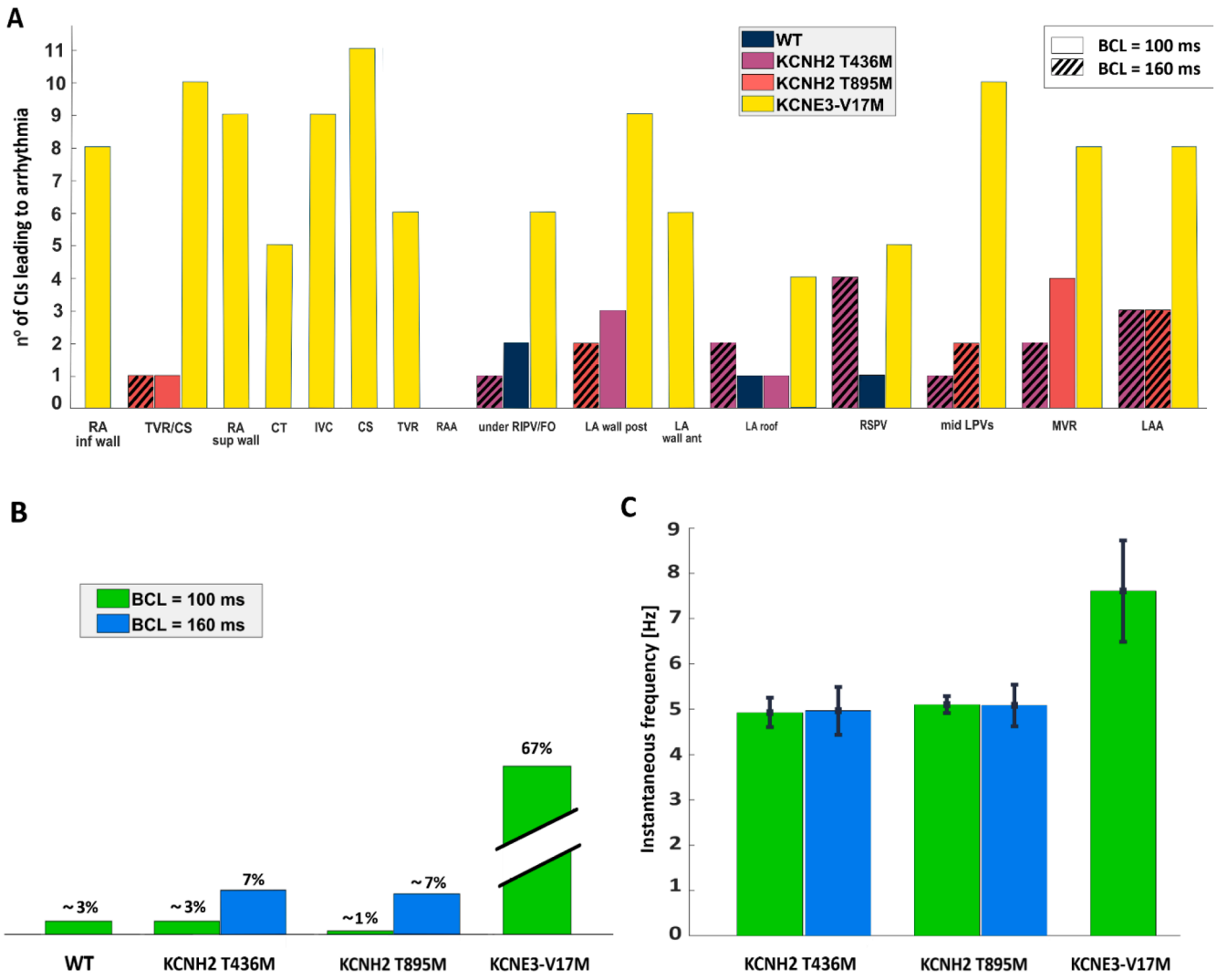

Fig. 5. Mutation effects on temporal vulnerability. A) Amount of CIs that elicited arrhythmic patterns represented by the sixteen EF locations and for the two BCLs used. The colour identifies the three mutations – KCNH2 T436M (purple), KCNH2 T895M (orange red), KCNE3-V17M (yellow) – and the healthy case, WT (dark blue). Results with S2-BCL = 100 are shown with full coloured bars, while results with S2-BCL = 160 ms are shown with coloured dashed bars. **B)** Percentage of the total number of generated arrhythmias for each case under study and for each BCL – 100 ms above the line in green and 160 ms below the line in light blue. **C)** Instantaneous frequency values expressed as mean and deviation standard for each mutation and BCL case resulted in sustained arrhythmic behaviour.

4. Discussion

4.1. Main findings

In this simulation study, the aim was to investigate the effects of three genetic mutations and to assess the atria susceptibility to mutation-induced forms of AF by using 3D patient-specific computational model of the human atria. Four versions of the Courtemanche unicellular electrophysiological model were employed; one for each mutation case simulated – KCNH2 T436M, KCNH2 T895M, KNCE3-V17M – and one for the healthy case scenario [17]. The 3D geometrical model of the atria was built from CT scans of a former AF patient and regional electrical and histological heterogeneities were implemented by scaling channel conductances and by accurately defining fibre orientations and conduction velocities [20,25]. After being stabilized at cellular and atrial level, the APD values were computed and categorized into the nine ionic models for the four cases under study to analyse the impact of each mutation on the electrophysiological properties of the myocyte. Then, sixteen uniformly distributed EF sites were defined onto the volume of the atrial mesh and an S1-S2 stimulation protocol was applied to mimic random ectopic bursts. The atrial vulnerability assessment to AF onset was carried out by analysing the outcomes of the application of such stimulation protocol on each EF site, considering eleven coupling intervals and two S2 BCLs.

The main findings are as follow: *(i)* During sinus rhythm, the main effect of the presence of the three mutations was the shortening of the APD_{90} values with respect to WT in all the nine ionic models. *(ii)* The APD_{90} mean values were mostly affected by the KCNE3-V17M mutation, while less impacted by the KCNH2 T895M and KCNH2 T436M mutations. In the presence of ectopic activity, when S2–BCL was set to 100 ms *(iii)* the genetic mutation leading to the highest susceptibility of the atria to AF was the KCNE3-V17M and arrhythmias were induced in 15 out of 16 stimulated EF locations. *(iv)* The KCNH2 T436M and KCNH2 T895M mutations revealed much less impact in arrhythmia outbreaks. On the other hand, when S2 BCL was set to 160 ms, *(v)* the mutations showing a highest impact of susceptibility to AF were the KCNH2 T895M and KCNH2 T436M mutations. Both of them similarly affected the vulnerability of the atria to fibrillatory events. *(vi)* Finally, the KCNE3-V17M mutation revealed no effect on atrial susceptibility with S2 BCL set to 160 ms. *(vii)* The majority of the arrhythmias were originated in the left atrium (60%). *(viii)* The arrhythmic events elicited in the presence of the KCNE3-V17M mutation were characterized by the formation of rapid

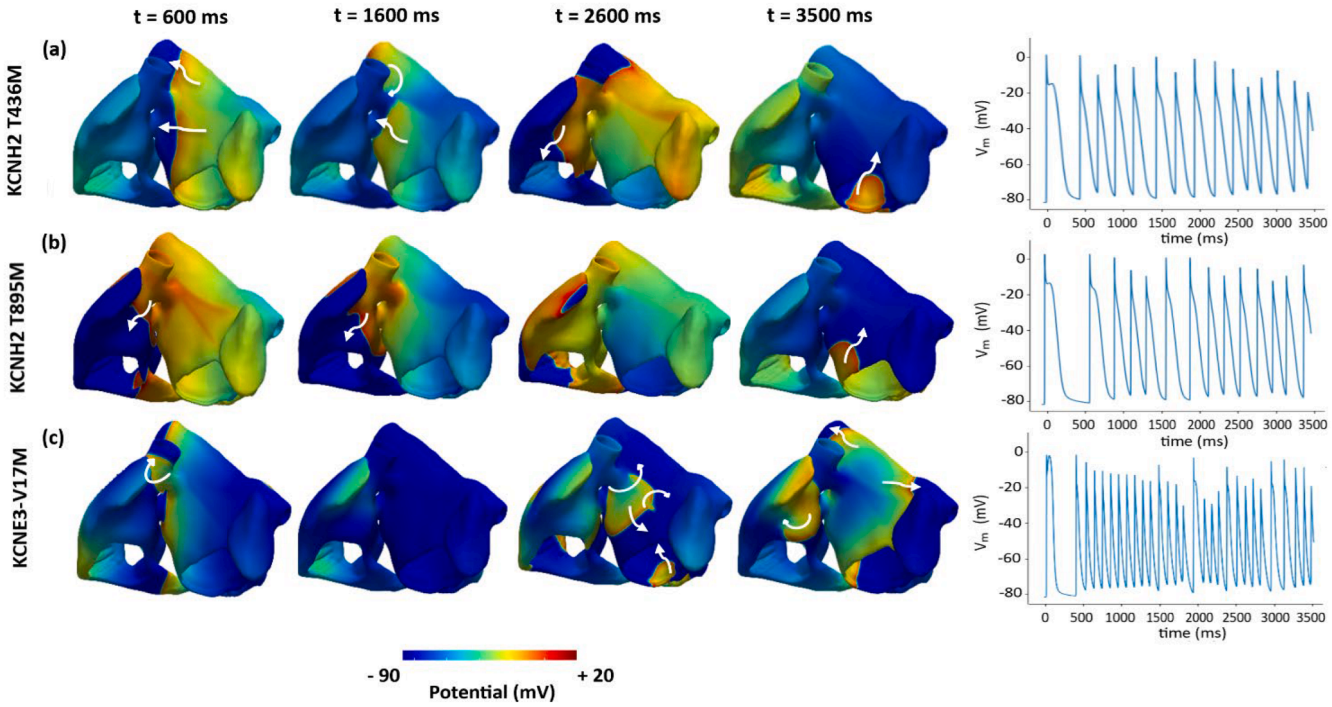

Fig. 6. Snapshot of scroll waves. Snapshots of spiral wave activity elicited by EF in mid LPV in the 3D patient-specific atrial model at (left) and the corresponding AP time courses recorded at a node located in the left atrium roof (right) for **(a)** KCNH2 T436M, **(b)** KCNH2 T895M and **(c)** KCNE3-V17M mutations. The coupling interval was equal to 0 ms for the KCNH2 T436M mutation and to 180 ms for the KCNH2 T895M mutation, the BCL being 160 ms in both cases, and to 20 ms for KCNE3-V17M mutation, the BCL being 100 ms. White arrows indicate the propagation direction of fibrillatory activity.

spiral waves moving around the atrial tissue with multiple re-entries, wave breaks and an overall chaotic electrical pattern with an instantaneous frequency mean of 7.6 Hz and a standard deviation of 1.12 Hz. Meanwhile, in the presence of the KCNH2 T436M and KCNH2 T895M mutations, the pattern of the scroll waves were stable and regular; the instantaneous frequency mean observed are within the range of 4.9 – 5.1 Hz with a standard deviation within 0.19 to 0.53 Hz.

To the best of our knowledge, this simulation study represents the first extensive and comprehensive investigation of the effects of genetic mutations acting on potassium channels using highly detailed 3D patient-specific human atrial models with realistic wall thickness, heterogeneous electrical properties and fibre orientation among atrial regions. The results of the computational study show that the KCNE3-V17M is the most arrhythmogenic mutant. It led to a strong reduction in the APD_{90} values with respect to the remaining mutations and to the WT (Fig. 3), and to a high onset of fibrillatory events regardless the pacing site, contrarily to the KCNH2 T436M and KCNH2 T895M mutations (Fig. 5A). The impact of the KCNH2 T436M and KCNH2 T895M mutations on the APD_{90} is moderate both in single cell [17] and in 3D studies; moreover, the heterogeneity of the APD_{90} among the nine models has a trend similar to the WT case, but with lower values. As a consequence, the generation of AF in such conditions is much more sensitive to the ionic model with respect to the KCNE3-V17M mutation. The coupling interval values that led to AF demonstrated that atrial substrate maintains its propensity and vulnerability to AF formation not only in proximity to the effective refractory period, but also in a delayed time window. All these differences highlight even more the role of the mutations on the generation of different type of substrate prone to AF. Our findings support and extend the results of our previous work where the pro-arrhythmogenicity of the KCNE3-V17M, KCNH2 T895M and KCNH2 T436M mutations was demonstrated on cellular and tissue scale, and proved that these pathological conditions play a fundamental role in increasing the predisposition of atrial substrate to be vulnerable to fibrillation. The results of this study provide further understanding of the intricated dynamics behind mutation-induced forms of AF by means of the use of detailed 3D mathematical models. The strategy here employed can eventually serves as first step into a targeted pharmaceutical treatment or into the definition of a patient-specific ablation procedure.

4.2. *Relevance respect to previous studies*

The vulnerability assessment of the atria to AF was carried out by considering many different sources of ectopic bursts and a wide range of coupling intervals. This technique allowed the evaluation of the influence of the cardiac regions to the generation of fibrillatory activity and to analyse the time window when such activity could be elicited. The stimulation protocol employed this study was an S1-S2 protocol, where the S2 is a train of 10 stimuli applied to the EF region at high frequencies. Rapid triggering is in fact considered as the main hypothesis of atrial fibrillation episodes onsets, favouring the propagation of spiral waves in presence of a substrate susceptible to re-entrant activities. On top of that, the presence of structural complexity and electrophysiological properties of atrial regions can help in the identification of areas where the probability to generate re-entry is demonstrated to be higher [2]. In clinical applications, decremental rapid pacing and bursts pacing have been frequently applied to evaluate the endpoint of a treatment, even though no fixed setups are followed, and the pacing locations are varied, usually among CS, PV, RA wall and the appendages [26–32]. Similarly, previous computational studies investigating permanent AF and fibrotic substrate have presented methods to investigate atrial vulnerability to AF inducibility mainly using decremental rapid pacing protocol and multiple ectopic sites uniformly distributed across the atria aiming at determining reliable ablation target [33,34]. Although the objective of the study is different, a very similar approach has been employed in this work. Our stimulation protocol was designed to reproduce a spontaneous realistic scenario of fibrillatory onset that could be considered relevant from the clinical point of view without aiming to reproduce the setups used in clinics. Moreover, this pacing method is applied to study the propensity to arrhythmia generation and

to investigate a large time window using eleven coupling intervals up to 200 ms. The results demonstrated that the substrate remains prone to AF initiation both close and far from the effective refractory period in most of the simulated cases. This is partially in line with the results described in [35,36] where an arrhythmia could be elicited with ectopic stimulations at the end of to the ERP and close to the ERP. However, simulations to study the permanence of the AF-prone substrate far from ERP were not considered in the abovementioned works.

Different previous studies investigated the impact of mutation-induced forms of AF and 3D computational models were used to perform simulations and evaluate the role of the mutations in initiating and sustaining arrhythmic activity. In Kharche [11,16], the effects of genetic mutations affecting I_{K1} and I_{Ks} were assessed in an electrically homogenous 3D geometry by pacing in a single point placed in the RA region and observing scroll waves evolution. Similarly in Imaniastuti and Zulfa [13,12], a left atrium mesh was used to perform 3D computer simulations and to assess the effects of the mutation affecting the I_{Ks} channel on an electrical homogeneous mesh and arrhythmia was induced by forcing an LA region back to resting potential and thus provoking a re-entry. On the contrary, our computational study represents an extensive examination of the impact of genetic mutations in potassium channels on a highly detailed 3D human atrial model specific to a patient. In this work the vulnerability of the atria is extensively examined and the effects of three gain-of-function mutations are evaluated by taking into account sixteen possible sources of ectopic bursts and eleven CIs. Moreover, the electrically heterogeneous 3D geometry enabled the possibility to investigate the effects and impact on the regional properties in the formation of fibrillatory activity.

4.3. Limitations

The impact of the three genetic mutations was assessed using a highly detailed 3D human atrial geometry, built from the CT scans of a former AF patient. Such realistic 3D model allows the personalization of the study, since the atria resulted slightly dilated; however, a more detailed understanding of the mutations' effects would be possible using other human atrial geometries or average model of healthy and dilated atria.

The stimulation protocol employed in this study on the 16 ectopic foci locations used two different BCLs, 100 ms and 160 ms. Applying the induction protocol with a much wider range of BCLs values would be helpful in the characterization of BCL dependence. However, this would results in a much more computational expensive studies. The two values chosen in this work can be considered representative as they are close to the ERP of the three mutant cell models. The designed stimulation protocol is able to reproduce spontaneous onsets that could be considered realistic and clinically relevant.

In this simulation study, the effects of the genetic defects were integrated by modifying the electrical dynamics of the ionic channels in a single cell. This represents the only change made to the model to include the mutant effects. No fibrotic substrate or conduction velocity reduction have been implemented to further characterize the 3D human atrial model. This decision can be considered acceptable and realistic in the assumption of an early-stage AF case; nevertheless, it is important to take into account that structural remodeling happens as a consequence of mutation related AF forms in long forms of AF [37,38].

Nevertheless, we believe these limitations do not alter or invalidate the main conclusions of this study.

5. Conclusions

In this study, the three gain-of-function mutations – namely, KCNH2 T895M, KCNH2 T436M, and KCNE3-V17M – were demonstrated to have pro-arrhythmogenic effects on complex 3D cardiac models. To the best of our knowledge, this represents the first extensive 3D in-silico study of the impact of genetic mutation on potassium channels. The use of a patient–specific 3D atrial geometry, the presence of heterogeneous electrical properties and realistic fibre directions allowed a truthful representation. The results showed the impact of the three mutants on the shortening of the APD_{90} values and the general increase in susceptibility of the atria to AF. Rapid and unpredictable scroll waves were observed when in the presence of the KCNE3-V17M mutation; more steady arrhythmic patterns were caused by the presence of the KCNH2 T436M and KCNH2 T895M mutations. Such findings support and build upon our previous research, further demonstrating the fundamental role of these pathological conditions in increasing the atrial substrate's vulnerability to fibrillation. This study contributes to the research on targeted treatment for individuals suffering from hereditary heart conditions that affect normal electrical functioning. Moreover, it gives a further understanding of the intricated dynamics behind mutation-induced forms of AF by means of the use of detailed 3D mathematical models. Our aim is to provide a foundation for a comprehensive examination of the complex relationships between genetic defects using advanced 3D mathematical models, which may result in future tailored drug treatment, or an ablation strategy specific to each individual patient.

6. Funding

This work was supported by the European Union's Horizon 2020 research and innovation program under the Marie Skłodowska-Curie gran agreement No. 766082 (MY-ATRIA project), by the Dirección General de Política Científica de la Generalitat Valenciana (PROMETEO/2020/043) and was partially funded by grant PID2022-140553OB-C41 funded by MICIU/AEI/10.13039/501100011033 and by ERDF/EU.

CRediT authorship contribution statement

Rebecca Belletti: Writing – review & editing, Writing – original draft, Validation, Methodology, Investigation, Formal analysis, Data curation, Conceptualization. **Joaquín Osca:** Writing – review & editing, Supervision, Methodology. **Lucia Romero Perez:** Writing – review & editing, Visualization, Validation, Supervision, Methodology, Formal analysis, Conceptualization. **Javier Saiz:** Writing – review & editing, Validation, Supervision, Resources, Project administration, Funding acquisition, Formal analysis, Conceptualization.

Declaration of competing interest

The authors declare that the research was conducted in the absence of any commercial or financial relationships that could be construed as a potential conflict of interest.

Acknowledgments

The authors thankfully acknowledge RES resources provided by Barcelona Supercomputing Center in MareNostrum5 (IM-2024-1-0010 and IM-2024-2-0015).

Supplementary materials

Supplementary material associated with this article can be found, in the online version, at doi:10.1016/j.cmpb.2024.108307.

References

[1] G. Hindricks, et al., 2020 ESC Guidelines for the diagnosis and management of atrial fibrillation developed in collaboration with the European Association for Cardio-Thoracic Surgery (EACTS), Eur. Heart J. 42 (5) (2021) 373–498, https://doi.org/10.1093/eurheartj/ehaa612.

[2] L. Staerk, J.A. Sherer, D. Ko, E.J. Benjamin, R.H. Helm, Atrial fibrillation epidemiology, pathophysiology, and clinical outcomes, Am. Hear. Assoc. Inc. 120 (9) (2017) 1501–1517, https://doi.org/10.1161/CIRCRESAHA.117.309732.
[3] J. Kornej, et al., Epidemiology of atrial fibrillation in the 21st century: novel methods and new insights, Circ. Res. (2020) 4–20, https://doi.org/10.1161/CIRCRESAHA.120.316340.
[4] J. Feghaly, P. Zakka, B. London, C.A. Macrae, M.M. Refaat, Genetics of atrial fibrillation, J. Am. Heart Assoc. 7 (2018) 1–15, https://doi.org/10.1161/JAHA.118.009884.
[5] A.A.Y. Ragab, G.D.S. Sitorus, B.B.J.J.M. Brundel, N.M.S. de Groot, The genetic puzzle of familial atrial fibrillation, Front. Cardiovasc. Med. 7 (2020) 1–8, https://doi.org/10.3389/fcvm.2020.00014.
[6] I.E. Christophersen, P.T. Ellinor, Genetics of atrial fibrillation: from families to genomes, J. Hum. Genet. 61 (1) (2016) 61–70, https://doi.org/10.1038/jhg.2015.44.
[7] L. Andreasen, J.B. Nielsen, M.S. Olesen, Genetic Aspects of lone atrial fibrillation : what do we know? Curr. Pharm. Des. 21 (5) (2015) 667–678, https://doi.org/10.2174/1381612820666140825143610.
[8] E. Savio-Galimberti, et al., SCN10A/Nav1.8 modulation of peak and late sodium currents in patients with early onset atrial fibrillation, Cardiovasc. Res. 104 (2) (2014) 355–363, https://doi.org/10.1093/cvr/cvu170.
[9] Q. Li, et al., Gain-of-function mutation of Nav1.5 in atrial fibrillation enhances cellular excitability and lowers the threshold for action potential firing, Biochem. Biophys. Res. Commun. 380 (1) (2009) 132–137, https://doi.org/10.1016/j.bbrc.2009.01.052.
[10] O. Dössel, M.W. Krueger, F.M. Weber, M. Wilhelms, G. Seemann, Computational modeling of the human atrial anatomy and electrophysiology, Med. Biol. Eng. Comput. 50 (8) (2012) 773–799, https://doi.org/10.1007/s11517-012-0924-6.
[11] S. Kharche, et al., Atrial proarrhythmia due to increased inward rectifier current (IK1) arising from KCNJ2 mutation - A simulation study, Prog. Biophys. Mol. Biol. 98 (2–3) (2008) 186–197, https://doi.org/10.1016/j.pbiomolbio.2008.10.010.
[12] I. Zulfa, E.B. Shim, K.S. Song, K.M. Lim, Computational simulations of the effects of the G229D KCNQ1 mutation on human atrial fibrillation, J. Physiol. Sci. 66 (5) (2016) 407–415, https://doi.org/10.1007/s12576-016-0438-3.
[13] R. Imaniastuti, H.S. Lee, N. Kim, J.B. Youm, E.B. Shim, K.M. Lim, Computational prediction of proarrhythmogenic effect of the V241F KCNQ1 mutation in human atrium, Prog. Biophys. Mol. Biol. 116 (1) (2014) 70–75, https://doi.org/10.1016/j.pbiomolbio.2014.09.001.
[14] A. Loewe, M. Wilhelms, F. Fischer, E.P. Scholz, O. Dössel, G. Seemann, Arrhythmic potency of human ether-à-go-go-related gene mutations L532P and N588K in a computational model of human atrial myocytes, Europace 16 (3) (2014) 435–443, https://doi.org/10.1093/europace/eut375.
[15] A.K. Heikhmakhtiar, A.T. Abrha, D.U. Jeong, K.M. Lim, Proarrhythmogenic effect of the L532P and N588K KCNH2 mutations in the human heart using a 3D electrophysiological model, J. Korean Med. Sci. 35 (29) (2020) 1–13, https://doi.org/10.3346/JKMS.2020.35.E238.
[16] S. Kharche, et al., Pro-arrhythmogenic effects of the S140G KCNQ1 mutation in human atrial fibrillation - insights from modelling, J. Physiol. 590 (18) (2012) 4501–4514, https://doi.org/10.1113/jphysiol.2012.229146.
[17] R. Belletti, L. Romero, L. Martinez-Mateu, E.M. Cherry, F.H. Fenton, J. Saiz, Arrhythmogenic effects of genetic mutations affecting potassium channels in human atrial fibrillation: a simulation study, Front. Physiol. 12 (May) (2021) 1–16, https://doi.org/10.3389/fphys.2021.681943.
[18] P.M. Boyle, S. Zahid, N.A. Trayanova, Towards personalized computational modelling of the fibrotic substrate for atrial arrhythmia, Europace 18 (2016), https://doi.org/10.1093/europace/euw358 pp. iv136–iv145.
[19] S. Rocher, L. Martinez, A. Lopez, A. Ferrer, D. Sanchez-Quintana, J. Saiz, A three-dimensional model of the human atria with heterogeneous thickness and fibre transmurality - a realistic platform for the study of atrial fibrillation, 2019 Comput. Cardiol. Conf. 45 (2019) 2019–2022, https://doi.org/10.22489/cinc.2019.380.
[20] A. Ferrer, et al., Detailed anatomical and electrophysiological models of human atria and torso for the simulation of atrial activation, PLoS ONE 10 (11) (2015) 1–29, https://doi.org/10.1371/journal.pone.0141573.
[21] M. Courtemanche, R.J. Ramirez, S. Nattel, Ionic mechanisms underlying human atrial action potential properties: insights from a mathematical model, Am. J. Physiol. -Heart Circ. Physiol. 275 (1998) 301–321, https://doi.org/10.1152/ajpheart.1998.275.1.H301.
[22] E. Grandi, et al., Human atrial action potential and Ca 2+ Model, Circ. Res. 109 (9) (2011) 1055–1066, https://doi.org/10.1161/circresaha.111.253955.
[23] R.F. Bosch, X. Zeng, J.B. Grammer, K. Popovic, C. Mewis, V. Kühlkamp, Ionic mechanisms of electrical remodeling in human atrial fibrillation, Cardiovasc. Res. 44 (1) (1999) 121–131, https://doi.org/10.1016/S0008-6363(99)00178-9.
[24] D. Dobrev, E. Wettwer, A. Kortner, M. Knaut, S. Schüler, U. Ravens, Human inward rectifier potassium channels in chronic and postoperative atrial fibrillation, Cardiovasc. Res. 54 (2) (2002) 397–404, https://doi.org/10.1016/S0008-6363(01)00555-7.
[25] L. Martinez-Mateu, et al., Factors affecting basket catheter detection of real and phantom rotors in the atria: a computational study, PLoS Comput. Biol. 14 (3) (2018) 1–26, https://doi.org/10.1371/journal.pcbi.1006017.
[26] M. Haïssaguerre, et al., Spontaneous initiation of atrial fibrillation by ectopic impulses originating in the pulmonary veins, Cardiol. Rev. 7 (2) (1999) 65, https://doi.org/10.1097/00045415-199903000-00006.
[27] P. Jaïs, et al., Long-term evaluation of atrial fibrillation ablation guided by noninducibility, Hear. Rhythm 3 (2) (2006) 140–145, https://doi.org/10.1016/j.hrthm.2005.11.012.
[28] M. Haïssaguerre, et al., Driver domains in persistent atrial fibrillation, Circulation 130 (7) (2014) 530–538, https://doi.org/10.1161/CIRCULATIONAHA.113.005421.
[29] H. Oral, et al., Noninducibility of atrial fibrillation as an end point of left atrial circumferential ablation for paroxysmal atrial fibrillation: a randomized study, Circulation 110 (18) (2004) 2797–2801, https://doi.org/10.1161/01.CIR.0000146786.87037.26.
[30] V. Essebag, et al., Non-inducibility post-pulmonary vein isolation achieving exit block predicts freedom from atrial fibrillation, Eur. Heart J. 26 (23) (2005) 2550–2555, https://doi.org/10.1093/eurheartj/ehi507.
[31] S. Kumar, J.M. Kalman, F. Sutherland, S.J. Spence, S. Finch, P.B. Sparks, Atrial fibrillation inducibility in the absence of structural heart disease or clinical atrial fibrillation: critical dependence on induction protocol, inducibility definition, and number of inductions, Circ. Arrhythmia Electrophysiol. 5 (3) (2012) 531–536, https://doi.org/10.1161/CIRCEP.111.968859.
[32] B. Richter, M. Gwechenberger, P. Filzmoser, M. Marx, P. Lercher, H.D. Gössinger, Is inducibility of atrial fibrillation after radio frequency ablation really a relevant prognostic factor? Eur. Heart J. 27 (21) (2006) 2553–2559, https://doi.org/10.1093/eurheartj/ehl307.
[33] P.M. Boyle, et al., Computationally guided personalized targeted ablation of persistent atrial fibrillation, Nat. Biomed. Eng. 3 (11) (2019) 870–879, https://doi.org/10.1038/s41551-019-0437-9.
[34] S. Zahid, et al., Patient-derived models link re-entrant driver localization in atrial fibrillation to fibrosis spatial pattern, Cardiovasc. Res. 110 (3) (2016) 443–454, https://doi.org/10.1093/cvr/cvw073.
[35] L. Azzolin, S. Schuler, O. Dössel, A. Loewe, A reproducible protocol to assess arrhythmia vulnerability in silico: pacing at the end of the effective refractory period, Front. Physiol. 12 (April) (2021) 1–14, https://doi.org/10.3389/fphys.2021.656411.
[36] R.B. Krol, S. Saksena, A. Prakash, I. Giorgberidze, P. Mathew, Prospective clinical evaluation of a programmed atrial stimulation protocol for induction of sustained atrial fibrillation and flutter, J. Interv. Card. Electrophysiol. 3 (19) (1999) 19–25, https://doi.org/10.1023/A:1009863220699.
[37] C.H. Roney, et al., In silico comparison of left atrial ablation techniques that target the anatomical, structural, and electrical substrates of atrial fibrillation, Front. Physiol. 11 (2020), https://doi.org/10.3389/fphys.2020.572874.
[38] A. Roy, et al., Identifying locations of re-entrant drivers from patient-specific distribution of fibrosis in the left atrium, PLoS Comput. Biol. 16 (9) (2020) 1–25, https://doi.org/10.1371/journal.pcbi.1008086.